

<https://doi.org/10.1038/s41612-024-00591-8>

The phase change in the annual cycle of sea surface temperature

Fucheng Yang¹ & Zhaohua Wu¹ ✉

In recent decades, many research efforts focused on global climate change, multidecadal, decadal, interannual variability, and the increasing extreme events of sea surface temperature. In contrast, the continuous evolution of the reference frame, the annual cycle of SST used to quantify the aforementioned variability and changes, has long been overlooked, resulting in difficulties in understanding the underlying physical mechanisms responsible for these variability and changes. In this study, we strive to bridge this gap on the phase changes in SST annual cycle. By devising a running correlation-based method, we can now quantify the non-sinusoidal shape of the evolving SST annual cycle, such as the advancing or delaying of summer and winter peaking times. It is revealed that the varying phases of summer or winter are more closely linked to multidecadal SST variability than to long-term climate change. Both the systematic shift of the phase and alterations in the annual cycle shape contribute to the phase changes, which explain 0.4~1.0 °C of monthly SST anomaly with respect to the climatological annual cycle in a multidecadal timescale. Furthermore, it is evident that the SST phases in historical simulations are better captured in winter than in summer and exhibit stronger variation compared with observation.

The Earth's climate system is highly nonlinear. When subjected to the annually periodic solar radiative forcing, the surface temperature typically exhibits a quasi-annually periodic evolution. This observed characteristic of such evolution has been documented in previous studies spanning decades¹⁻⁹. Moreover, it has been demonstrated that considering the amplitude-frequency modulated annual cycle (MAC) can significantly impact the physical interpretations of various phenomena depending on deseasonalization methods¹⁰, such as the changes in the frequency of El Niño-Southern Oscillation (ENSO) and its phase-locking to the annual cycle¹¹⁻¹³, the re-emergence of sea surface anomalies in the North Atlantic Ocean¹², and the reconciliation of differences in decadal variability between summer and winter climates¹².

Another area where the consideration of MAC can enhance our understanding of physical mechanisms is the study of highly damaging weather and climate extremes. Recent reports have highlighted an increase in the frequency of extreme weather and climate events¹⁴⁻¹⁷. Among these, marine heatwaves (MHW) have attracted significant research attention¹⁸⁻²⁰, owing to their potential impact on communities and ecosystems²¹⁻²⁵. It has been argued that changes in mean sea surface temperature (SST), rather than its variance, are the dominant drivers of MHW changes¹⁹. If the climate shifts toward warmer conditions, the probability of extremely hot

temperature occurrence may increase due to the narrower distribution of SST anomalies²⁶. In most of the aforementioned studies, quantification of extremes utilized weather and climate anomalies with respect to the repetitive climatological annual cycle, without accounting for amplitude and phase variations in individual year's annual cycles. While this approach provides a consistent reference framework and is convenient, it hinders our understanding of the diverse physical mechanisms underlying extreme events.

This issue is illustrated in Fig. 1, which plots the 31-day running means of SST in a mid-latitude region for three selected years and their corresponding anomalies with respect to the climatological annual cycle and the individual year running means, respectively. (*Hereafter*, the anomaly with respect to the climatological annual cycle is referred to as traditional anomaly.) There are several key features of this figure:

- (1) The low-passed SST, primarily dominated by SST annual cycle components, exhibits summer and winter peaking times at significantly different temporal locations. For example, the difference in summer peaking days between 2007 and 2009 exceeds 30 days.
- (2) The SST annual cycle can be highly non-sinusoidal, with the warming season lasting approximately 150 days and the cooling season extending for around 215 days in 2009.

¹Department of Earth, Ocean and Atmospheric Science & the Center for Ocean-Atmospheric Prediction Studies, Florida State University, Tallahassee, FL, USA.

✉ e-mail: zww@fsu.edu

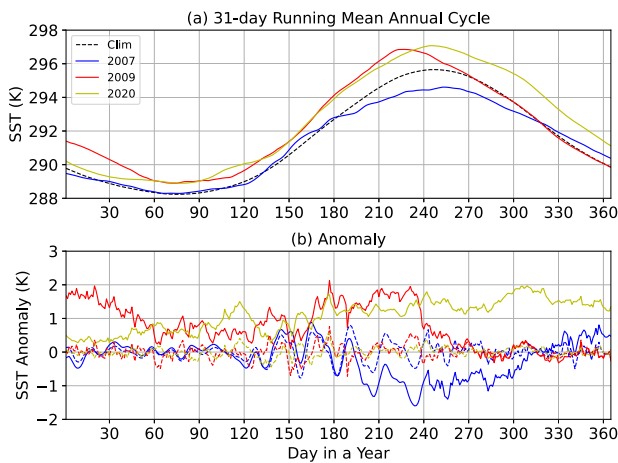


Fig. 1 | Examples of SST annual cycles and corresponding anomalies. **a** 31-day running mean annual cycle (blue for 2007, red for 2009, yellow for 2020, and black for climatology) and **b** anomalies with respect to climatology (solid lines) and to running mean annual cycle (dashed lines) in a region of the eastern North Pacific Ocean (150–140°W, 30–40°N).

- (3) Traditional anomalies (defined using SST data from 1940 to 2020) are close throughout day 60 to day 240 for the years 2009 and 2020, but anomalies with respect to individual running means display minor and highly random fluctuations.

When defining extremes using the absolute threshold values of SST (e.g., SST values larger than 30 °C in the western Tropical Pacific Ocean), the identification of extremes is irrelevant to the definition of anomaly and remains unaffected. However, estimating the probability of extreme occurrence in this case becomes challenging due to reduced randomness and a lack of independent samples. On the other hand, if extremes are defined using anomalies with respect to running the mean annual cycle, the smallness of these anomalies contributes less to quantifying extremes, consistent with the findings of Frölicher & Laufkötter²⁶ and Oliver¹⁹. Therefore, understanding SST extremes hinges not on synoptic SST variability but rather on the varying annual cycle and longer timescale SST variability.

The annual cycle stands out as the dominant quasi-periodic component of SST, and its amplitude is almost an order larger than the sum of all SST interannual and longer timescale variability and change. Previous studies also reported systematic shifts of annual cycle both on land and oceans in past decades^{5,6,10,13}. Surprisingly, despite its significance, climate scientists have historically understood other timescales of SST variability and change better than this predominant component. A recent study systematically investigated the physical mechanisms shaping the SST annual cycle²⁷. In their research, the authors developed a simple energy budget model that incorporated the seasonally varying heat capacity of the oceanic mixed layer, successfully reproducing both the phase and amplitude of the SST annual cycle in mid-latitude oceans and the Southern Ocean. However, the study of Yang & Wu did not extend their focus to how SST annual cycles have evolved alongside ongoing global climate change.

The primary objective of this study is to address this information gap by analyzing widely recognized SST reanalysis data. The focus will be directed toward the variability and changes in the shape of the SST annual cycle over the mid-latitude North Pacific Ocean and North Atlantic Ocean. To achieve this objective, we have devised a methodology to bypass the simultaneous change in the phases of summer and winter, a drawback often tied to Fourier-based annual cycle fitting.

Results

Our analysis focuses on the variability and changes of SST annual cycle phases in mid-latitude oceans. Previous studies used only one trigonometric component with a 365-day period to fit the data year by year. They obtained

annual cycles and then analyzed the phase of this trigonometric component. However, the annual cycles, as shown in Fig. 1a, exhibit high asymmetry, including differences in the duration of warming and cooling seasons (also see Supplementary Fig. 1). The trigonometric fitting method ignores this asymmetry and cannot accurately resolve the phase shift of either summer or winter.

In this study, we have developed a method to separately determine the peaking timing of summer and winter for individual annual cycles, effectively addressing the limitations of prior research. The asynchronous change in the summer and winter phases represents the asymmetry of SST annual cycle. Please note that the *phase* and the *peaking time* (or *date*) are the same in this study but differ from the timing of absolute maximum or minimum. The datasets under analysis comprise reanalysis data, specifically HadISST²⁸ and ERA5 SST²⁹, along with model data from CMIP6 historical simulations³⁰. Our devised method, when employed to ascertain the phase variability of the SST annual cycle, exhibits robustness and is not sensitive to synoptic variability. For a more comprehensive understanding of our approach and the data employed, please refer to Methods.

Summer and winter phases variability and change

Figure 2 presents the linear trends of ERA5 SST phase from 1940 to 2021 for individual grids with a size of 5° × 5°. Similar spatial patterns of phase shift trends are observed in the corresponding HadISST linear trends, as depicted in Supplementary Fig. 2, suggesting the adaptability of our method. In terms of annual averages, our method's results and the traditional trigonometric function fitting^{2,6} yield consistent findings (Fig. 2a and b). Both methods show that the interiors of the mid-latitude North Pacific Ocean and North Atlantic Ocean are experiencing delayed seasons while surrounding regions are advancing. Over the past decades, the phase change has reached up to 1.0 days per decade.

Notably, there are differences between the patterns of summer and winter phase trends, as shown in Fig. 2c and d. The change in winter peaking time is more pronounced than that in summer. Additionally, the spatial patterns of summer and winter trends differ significantly, particularly in the North Atlantic Ocean. The pattern correlation between the summer and winter patterns is approximately 0.67, suggesting that one pattern can only explain 45% of the variance in the other. This implies that traditional trigonometric function fitting can account for less than half of the phase change in the SST annual cycle, with the remaining larger portion of the trend being associated with the enhancement of annual cycle asymmetry, i.e., a longer or shorter SST increasing (or decreasing) season.

In addition to the long-term trends, the SST phases exhibit more pronounced multidecadal variations, as illustrated in Fig. 3. These variations reach magnitudes exceeding 3.0 day per decade, which is thrice as large as the long-term trends. Furthermore, the multidecadal variability displays significant spatial differences: while the mid-latitude North Pacific Ocean experiences an advancing peaking time of a season, the mid-latitude North Atlantic Ocean shows a delay, indicating a strong contrast between the two ocean basins. This contrast is supported by a correlation value of −0.56 between the low-passed variability (represented by the blue and red curves in Fig. 3a) in the most prominent phase shift regions with statistically significant marks. This feature is most pronounced from 1960 to 1990 (see more details for other decades in Supplementary Figs. 3 and 4). During this period, the SST annual cycle shifted towards later seasons in the eastern North Pacific Ocean and toward earlier seasons in the western North Atlantic Ocean. Interestingly, the spatial patterns of summer and winter variability appear to closely resemble each other while the summer phase trend is strongest in the North Pacific Ocean and the winter phase trend is strongest in the North Atlantic Ocean, again suggesting the change in annual cycle asymmetry.

Phases and anomalies

To illustrate how phase shift and shape change in SST annual cycle impact traditional anomaly values, we first make an estimation based on a zig-zag-shaped annual cycle of 360 days. In this annual cycle, both the warming and

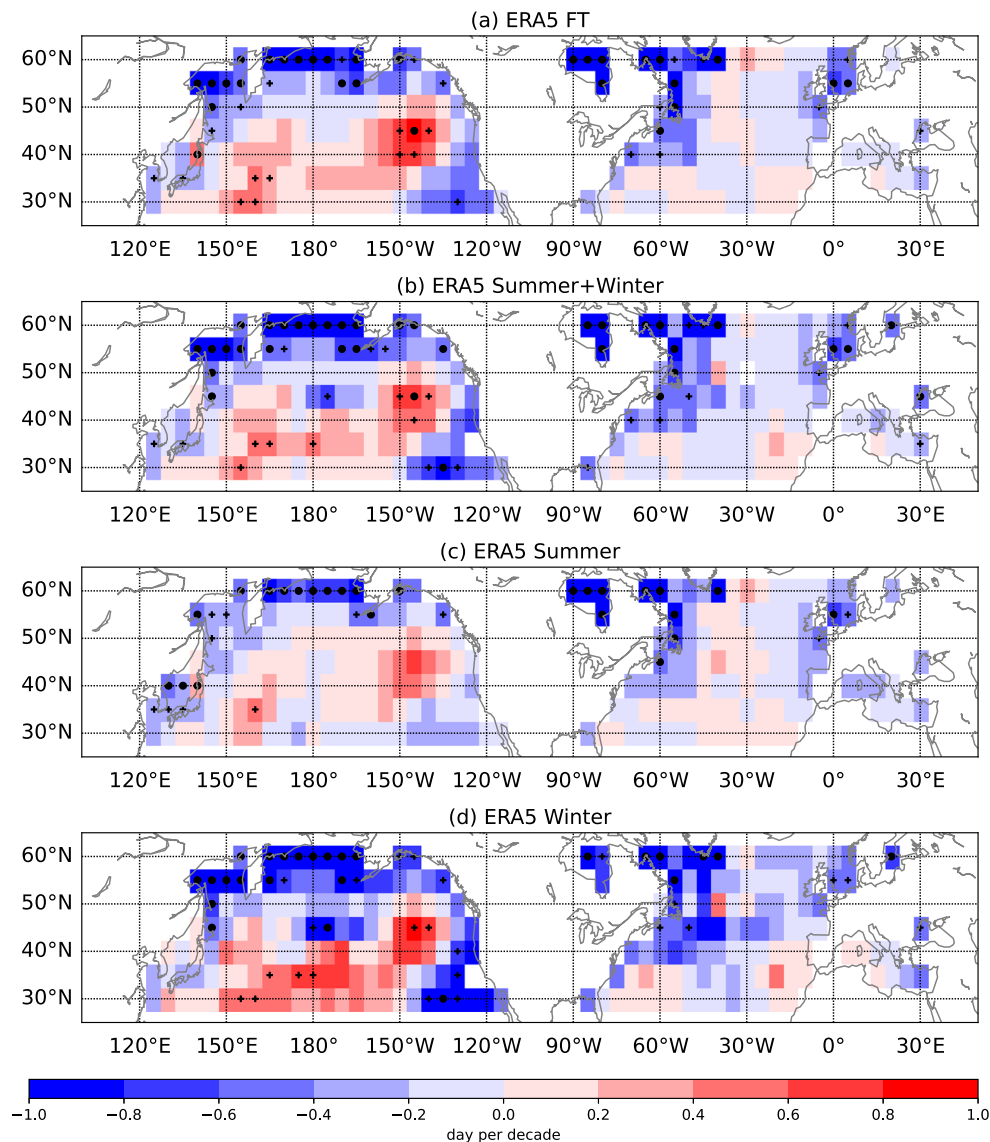


Fig. 2 | The trends of SST phase during 1940–2021 for ERA5. The phases are obtained by a Fourier transform and **c, d** running correlation. **b** represents the averaged phases of summer and winter from **c** and **d**. Markers “+” and “•” represent a significance judged using 95% and 99% confidence intervals, respectively.

cooling seasons last for 180 days, with a minimum–maximum temperature difference of 10 °C, a typical value for the amplitude of the mid-latitude SST annual cycle. The corresponding warming and cooling rates have a magnitude of about 0.06 °C per day. If this annual cycle is systematically delayed or advanced by 10 days, it results in almost a half-year SST change of $\sim \pm 0.6$ °C. The change in the shape of the annual cycle can also result in a similar anomaly. Suppose the winter peaking time unchanged, when the warming season is shortened by 10 days and the cooling season is prolonged by 10 days, a ± 0.6 °C anomaly is introduced before and after summer peaking time. Additionally, if we replace the straight-line warming and cooling seasons with a more realistic mode, such as sinusoidal function, the temperature anomaly can be up to 0.86 °C because the temperature change rates in spring and autumn are larger than the linear rates in the zig-zag shaped mode.

It is important to note that this simple estimation does not encompass the influence of interannual SST variation because 10-day phase shift is a typical value of regional averaged phase change in two or three decades suggested in Fig. 3. If we also consider the year-to-year variability in the annual cycle, the traditional anomaly attributed to annual cycle variability and changes can reach up to 2 °C (see the temperature difference during autumn and winter between year 2009 and 2020 in Fig. 1a).

These arguments are applicable to real-world scenarios. In Fig. 4, we illustrate the regression of phase delay to the traditional anomaly of SST observed in different months. This regression reflects the systematic alteration of traditional anomaly associated with changes in summer or winter peaking time. Even though the calculations are conducted for individual $5^\circ \times 5^\circ$ grids, the regressions consistently exhibit one-signed values over the whole mid-latitude oceans, indicating a systematic link between the change in the shape of the annual cycle and the traditional anomaly.

This result is comprehensible: the delay in summer peaking time reflects a lagging warming/cooling of SST compared to the climatology prior to/post the summer peak time, contributing to a negative traditional anomaly in June and July (Fig. 4a) and a positive traditional anomaly in October and November (Fig. 4b). Similarly, the delay in the winter phase contributes to a positive traditional anomaly in December and January (Fig. 4c) and a negative traditional anomaly in March and April (Fig. 4d). These regressions suggest that a 10-day delay or advance in the summer peaking time can result in an absolute value of 0.4–1.2 °C in traditional anomaly in neighboring months, which is consistent with the above estimates. In the Supplementary, we also present the correlation maps between the delay of summer or winter peaking time and the traditional anomaly. The absolute correlation coefficients fall in the range of 0.2–0.7 (see Supplementary Figs. 5

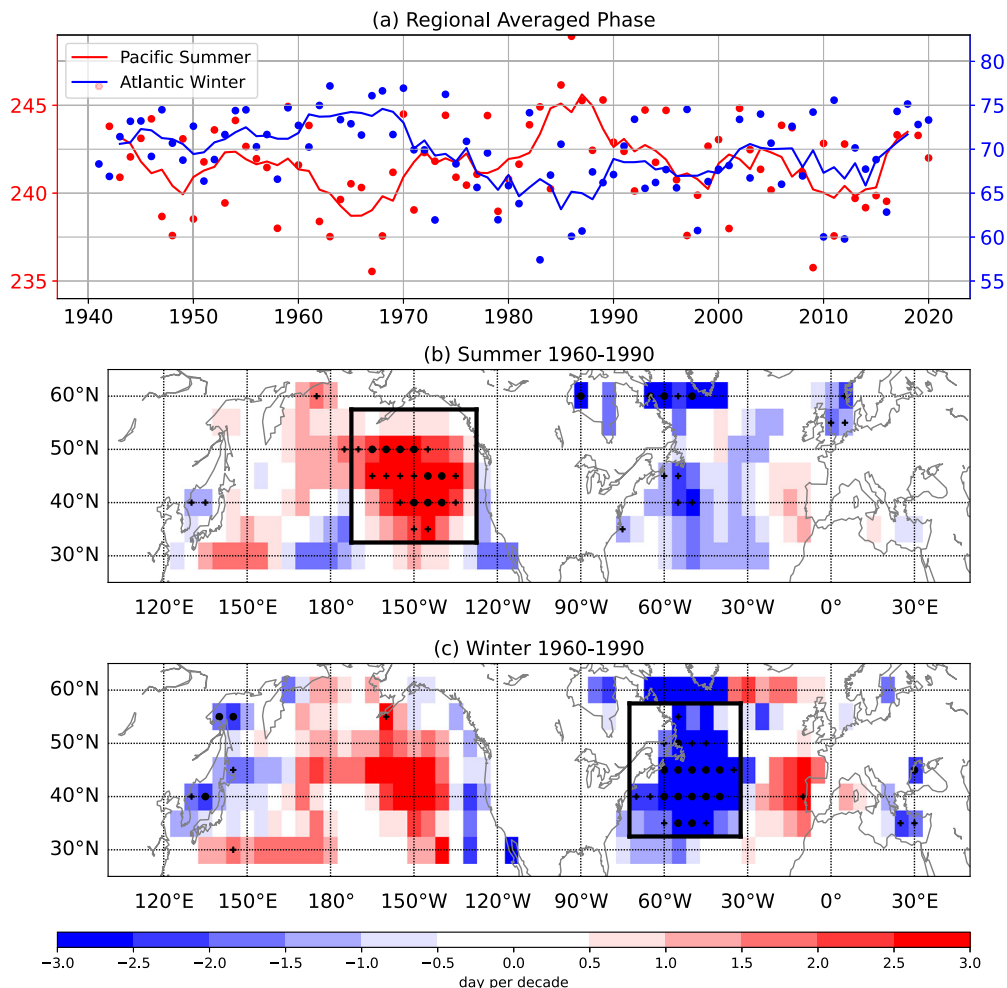


Fig. 3 | Multidecadal variation of SST phase from ERA5. **a** The time series of regional averaged summer phase in the North Pacific Ocean (red) and winter phase in the North Atlantic Ocean (blue), and the SST phase trends in **b** summer and

c winter during 1960–1990. Dots and curves represent the phases of individual years and 5-year running means, respectively. Two domains are denoted by black boxes in **b** and **c**. Significance is denoted by markers, as in Fig. 2.

and 6), suggesting that the annual cycle delay/advance can explain up to 40% of the traditional anomaly.

Annual cycle phases in CMIP6 historical simulations

Currently, climate studies heavily rely on climate system models. In this study, we also examine whether summer and winter phases in CMIP6 historical simulations are consistent with those in reanalysis data. We analyze a total of 13 climate models, each containing 10 historical runs. For each individual ensemble members, we determine the summer and winter peaking times using the same method described in the Methods section. Similar to those shown in Fig. 3a for ERA5 SST, once we obtain the summer and winter peaking times, we separate them into two components: the low-frequency part, obtained by the 11-year running mean, and the high-frequency part, the remained anomaly from the running mean.

The results are presented in Fig. 5. Most of these historical simulations capture the climatological peaking time, with the peaking dates deviating from those of ERA5 SST by less than 15 days (Fig. 5a, b). The majority of models with their ensemble runs exhibit larger variability in peaking times for both summer and winter when compared to observation on decadal to multidecadal timescale (Fig. 5c). Further analysis of the ratio between low-frequency and high-frequency variability in both seasons indicates that most ensemble members have smaller ratios than ERA5 SST. This suggests that, in CMIP6 models, the systematic shift or change in phases (reflected by the low-frequency part of peaking time variability) is often overshadowed by the substantial high-frequency variability or, in some cases, underestimated. In

Supplementary, we also demonstrate that the low-frequency phases of individual ensemble members can vary significantly in intra-model correlations (see Supplementary Fig. 8), and disagree with the results of ERA5 SST (see Supplementary Fig. 7).

Discussion

In this study, we analyze the variability and changes in the summer and winter phases. We demonstrate that the SST annual cycle in many regions of the northern mid-latitude oceans not only exhibits systematic phase delay or advance but also experiences a change in its shape associating with asymmetry. Both the systematic shift of the phase and alteration in the annual cycle shape contribute to the phase changes calculated by running correlation. The winter peaking times have advanced during the recent 80 years in the ocean regions adjacent to land, while the mid-latitude interior oceans, particularly the North Pacific Ocean, exhibit an opposite trend. The changes of peaking time are more pronounced in multidecadal timescale than in the long-term trend, and are asynchronous in summer and winter implying a change in the shape of SST annual cycle in addition to the systematic phase shift. Furthermore, it is evident that most CMIP6 models project a bias within 15 days in the climatological SST phase compared with observation. However, the impact of the temporal resolution of data on our results needs further investigation.

These results have significant implications for climate studies. Most research on climate variability and change typically begins with anomalies relative to a presupposed repetitive climatological annual cycle. However,

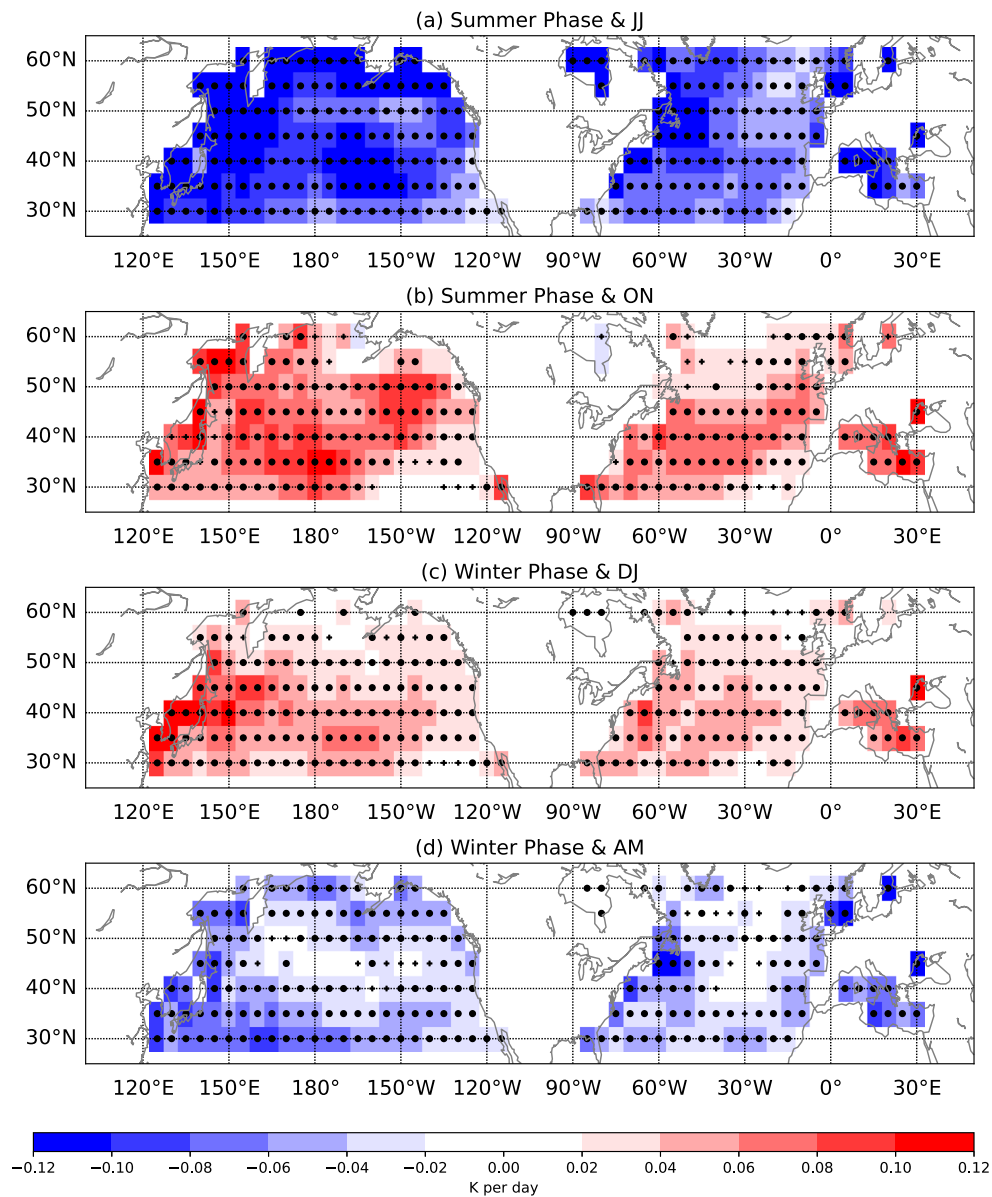


Fig. 4 | Regression of SST traditional anomaly on phases during 1940–2020 in ERA5 dataset. a, b Summer phases and SST before (June and July) and after summer peaking time (October and November). c, d Winter phases and SST before

(December and January) and after winter peaking time (April and May). Significance is denoted by markers, as in Fig. 2.

when the annual cycle changes significantly over time, the drawbacks of using a traditional repetitive annual cycle as the reference frame to define anomaly emerge for climate variability and change studies^{8,31,32}. This is particularly relevant given that up to 1 °C of the traditional anomaly can be attributed to phase changes of annual cycle in multidecadal timescale. Since the dynamical origin of the annual cycle, as revealed by Yang & Wu²⁷, differs from widely known explanations for major climate modes in terms of traditional anomaly, understanding the variability and changes in the annual cycle may offer a viable means of comprehending climate change.

Analysis of CMIP6 simulations also provides insights into model development. There has been a wide debate in previous studies regarding whether global climate models lack the sensitivity to accurately reproduce observed climate variability^{33–37}. The strength of interannual variability in CMIP6 SST phases is comparable with or slightly larger than in observation, but their variability of decadal to multidecadal timescale is much weaker. This result suggests that most models are sensitive enough to potential forcing in the SST annual cycle. However, they may lack adequate coupling between ocean and atmosphere or between regional and global climate to

accurately simulate decadal to long-term changes. While the simulated temperature of many models aligns with observations in terms of global and annual averages, the failure to model its annual evolution may result in a deficiency in interactions between regions.

As mentioned earlier, many studies employ the probability density function of weather/climate anomalies to quantify extreme weather/climate events. Due to the slow progression of the annual cycle relative to weather variability, such obtained anomalies often contain a component related to the time-varying annual cycle, especially in oceans. This results in prolonged periods of anomalies dominated by positive or negative values, rendering the traditional anomaly highly non-random. In such cases, the use of probability density functions becomes less effective, and it becomes challenging to establish a clear physical connection between the probability density function and the underlying mechanisms responsible for weather/climate extremes. If the portion of the anomaly associated with changes in the annual cycle can be isolated or extracted, the probability density function approach may be founded on a more robust statistical basis.

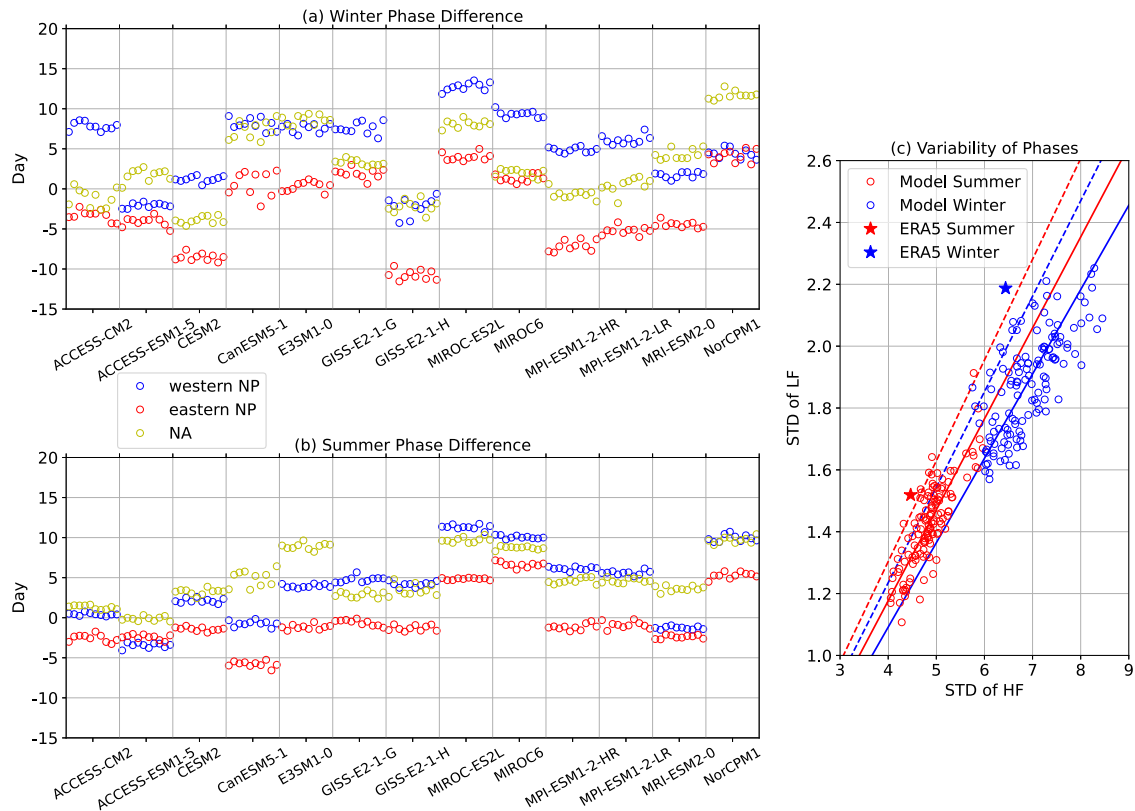


Fig. 5 | Comparison between modeled and ERA5 SST phases. **a, b** Difference of averaged phase in three regions: western North Pacific Ocean (blue), eastern North Pacific Ocean (red), and North Atlantic Ocean (yellow). The 10 circles for each model and each region represent results from 10 ensembles separately. Positive values represent lagging with respect to observation. **c** Variability of high-frequency and low-frequency components of phases. Two components are separated by 11-

year running mean. Markers open circle and star denote results from simulations and ERA5 SST, respectively. Solid lines represent the averaged standard deviation ratio of high-frequency and low-frequency components in ensembles, and dashed lines represent the departure of double inter-ensemble standard deviation (95% confidence interval) from the solid lines. Red color for the summer phase and blue for winter.

Methods
Data

The SST reanalysis data utilized in this study is from the Hadley Centre Sea Ice and Sea Surface Temperature dataset (HadISST)²⁸ and the 5th generation of European Centre for Medium-Range Weather Forecasts (ECMWF) Reanalysis (ERA5)²⁹. HadISST provides monthly data on 1° × 1° grids, which we linearly interpolate to generate daily data. On the other hand, ERA5 SST offers daily data on 1° × 1° grids, and we employ a 31-day running mean to filter out synoptic scale variability. Both datasets are further averaged within 5° × 5° boxes to attain smoother annual cycles. Additionally, in leap years, the 60th day is omitted, resulting in each year containing 365 days.

This study incorporates 130 historical simulations from 13 models (10 ensemble members from each model) in the Coupled Model Inter-comparison Project Phase 6 (CMIP6) to explore the internal variability of model climate (see Supplementary Table 1 for more details). Please note that many models do not contain complete ensemble members with r1–r10. The participating models encompass ACCESS-CM2, ACCESS-ESM1-5, CESM2, CanESM5-1, E3SM1-0, GISS-E2-1-G, GISS-E2-1-H, MIROC-ES2L, MIROC6, MPI-ESM1-2-HR, MPI-ESM1-2-LR, MRI-ESM2-0, and NorCPM1. The monthly SST data from these simulations are processed in a manner consistent with the approach used for HadISST to determine the phase of the annual cycle.

The original temporal range of HadISST is 1870 to date, ERA5 SST 1940 to date, and CMIP6 1850 to 2014 (two ensembles of E3SM-1-0 end in 2011 and 2013, respectively). When considering results from observations, we utilized data between 1940 and 2021. In the comparison of phases from observations and simulations, we selected the common temporal domain of

1940 to 2010. As illustrated in Supplementary Figs. 7 and 8, the multidecadal variability in CMIP6 historical simulations is contributed more by internal variability in different ensembles. We verified that the main conclusions related to this comparison are not sensitive to the selections of the comparison period as long as they are a few decades or longer. The linear trend utilized in this study is the least-squares fit, a common method to fit a straight line through the data. The 95% and 99% statistically significant testing is assessed by a one-sample *t* test.

Phases

Two methods are applied to compute phase of annual cycle in this study. The traditional phase of the annual cycle is computed by Fourier transform as in ref. 6:

$$a = \frac{1}{365} \sum_{n=1}^{365} e^{2\pi i n / 365} X'(n), \tag{1}$$

$$Y(n) = 2\text{Re}(ae^{-2\pi i n / 365})$$

where *n* is the date in a year (1 ≤ *n* ≤ 365), *X'*(*n*) SST of one year (it is a part of the original time series of SST, *X*(*t*)), *Y*(*n*) the annual harmonic in Fourier transform, and *a* the Fourier coefficient. The phase is defined as the timing of the maximum in *Y*(*n*).

The Fourier-based traditional method is quite rigid, e.g., having a trigonometric function of 365 days and an equal temporal spanning warming and cooling seasons. This rigidity cannot resolve the asymmetric of the seasonal cycle. For this reason, we devise here a method that is based on the running correlation for the purpose of determining the timings of summer peak and winter trough separately. This method is similar to traditional

wavelet transform except we use summer/winter characteristic function to replace the mother wavelet. By sliding the window, we obtain the largest correlation point and designate that point as either a summer peak or winter trough. The details of the method are as follows: First, a long-term mean (or climatological) annual cycle, X_0 , is obtained at each grid:

$$X_0(n) = \frac{1}{K} \sum_{k=0}^{K-1} X(n + 365k), \quad (2)$$

where K is the number of years in SST time series. Then, the seasonal characteristic function is defined from X_0 . For example, if the summer maximum temperature occurs at day 240 and the length, L , of the characteristic function is selected as 181 days, $X_0(n)$ ($150 \leq n \leq 330$) is the characteristic function of summer (see Supplementary Fig. 9a). Once the characteristic function is selected, correlation coefficient can be computed between the function and each piece of X :

$$Z(t) = \text{CORR}(X_0(n), X(t)), \quad (3)$$

where t is the day in decades, $L = 181$, $150 \leq n \leq 330$, and $t - (L - 1)/2 \leq t \leq t + (L - 1)/2$. Thus, in $Z(t)$, the timing of the maximum in each year is defined as the phase of summer (Supplementary Fig. 9b). Please note that two criteria are applied to determine whether this timing is effective: (1) the correlation coefficient corresponding to this timing must be larger than 0.9 and (2) the departure of this timing to the date of maximum in climatological annual cycle is less than 45 days. Grids with a number of ineffective phases over 30% of the whole period are masked. Similarly, if the winter minimum is at day 60 and $L = 181$, the winter characteristic function is $X_0(n)$ ($-30 \leq n \leq 150$) (there is negative n because X_0 is considered as a periodic function). The phase of winter is defined from the correlation coefficient between the winter characteristic function and each piece of $X(t)$.

In the analysis of SST annual cycle, the focus on phase arises from the interest in understanding whether seasons shift to earlier or later times. This leads to the fundamental question of how seasons are defined. In the context of annually evolving SST, the most prominent feature is the high temperature in summer and low temperature in winter, with spring and autumn serving as transition seasons. With an implicit assumption that the SST annual cycle does not dramatically change its shape, the climatological annual cycle can still be considered a reasonable reference shape of the SST annual cycle. If we take the wavelet analysis as analog, this shape is an adaptive mother wavelet of the annual cycle determined by SST data themselves. Since the running correlation method is used only for the determination of the timings of the annual cycle peak and bottom, the selection of the window length is a compromise between avoiding the effect of the asymmetry of the annual cycle and reducing the sensitivity caused by the residue sub-seasonal variability. We tested various widths of this running correlation window and the optimal window size of this is about one-half year. Since our data has a daily resolution, we maximize the resolution by selecting a running step of 1 day in the determination of the peak and bottom timings in running correlation.

The purpose of applying 31-day running mean, as well as a $5^\circ \times 5^\circ$ box average, is to reduce the effect of fast-fluctuating synoptic scale variability, which is often considered weather noise, and to correct the potential large contrast of the effect of the reminder synoptic variability of neighboring grids in the determination of the annual cycle. This spatiotemporal smoothing can lead to the phase of the SST annual cycle being unique. As illustrated in Supplementary Fig. 9c, the results from the selections of different widths of the running mean window only contain negligible differences if the window width is greater than 7 days and less than 60 days for the regions that our study focuses on, suggesting that the results from running correlation are robust. However, when we study the land surface temperature, which will be reported elsewhere, the sensitivity of the phase determination to a small temporal running mean window (e.g., <2 weeks)

increases. A selection of 31-day would put us in a uniform methodological framework when we analyze the surface temperature annual cycle over the whole globe.

Analyzing the timing of maximum or minimum temperature provides a logically clear definition that works well for climatological annual cycles⁹. However, the reason we determine the timing of peaking using the running correlation method rather than directly diagnosing from the 31-day running mean is that the 31-day running mean may contain a portion of high-frequency variability, which even features multiple local maximums within a short period in summer, for example. If the maximum of the 31-day running mean is used to determine the peaking phase of the annual cycle, the peak timing does not reflect the relatively slower evolution of the annual cycle phase. Supplementary Fig. 9c exhibits the unrealistic phase fluctuation when it is diagnosed from the 31-day running mean using the absolute maximum-minimum method.

Data availability

In this study, we used ERA5, HadISST, and CMIP6 historical data. They can be accessed from (1) <https://cds.climate.copernicus.eu/cdsapp#!/dataset/reanalysis-era5-single-levels>, (2) <https://www.metoffice.gov.uk/hadobs/hadisst/>, and (3) <https://pcmdi.llnl.gov/CMIP6/>, respectively. Derived data supporting the findings of this study are available from https://github.com/fcyang58/Changing_Annual_Cycle and the corresponding author upon reasonable request.

Code availability

The source codes for the analysis of this study are available from https://github.com/fcyang58/Changing_Annual_Cycle and the corresponding author upon reasonable request.

Received: 16 November 2023; Accepted: 9 February 2024;

Published online: 27 February 2024

References

- Loon, H. V., Kidson, J. W. & Mullan, A. B. Decadal variation of the annual cycle in the Australian dataset. *J. Clim.* **6**, 1227–1231 (1993).
- Thomson, D. J. The seasons, global temperature, and precession. *Science* **268**, 59–68 (1995).
- Gu, D., Philander, S. G. & McPhaden, M. J. The seasonal cycle and its modulation in the eastern tropical Pacific Ocean. *J. Phys. Oceanogr.* **27**, 2209–2218 (1997).
- Pezzulli, S., Stephenson, D. B. & Hannachi, A. The variability of seasonality. *J. Clim.* **18**, 71–88 (2005).
- Wallace, C. J. & Osborn, T. J. Recent and future modulation of the annual cycle. *Clim. Res.* **22**, 1–11 (2002).
- Stine, A. R., Huybers, P. & Fung, I. Y. Changes in the phase of the annual cycle of surface temperature. *Nature* **457**, 435–440 (2009).
- Dwyer, J. G., Biasutti, M. & Sobel, A. H. Projected changes in the seasonal cycle of surface temperature. *J. Clim.* **25**, 6359–6374 (2012).
- Qian, C. & Zhang, X. Human influences on changes in the temperature seasonality in mid-to high-latitude land areas. *J. Clim.* **28**, 5908–5921 (2015).
- Donohoe, A., Dawson, E., McMurdie, L., Battisti, D. S. & Rhines, A. Seasonal asymmetries in the lag between insolation and surface temperature. *J. Clim.* **33**, 3921–3945 (2020).
- Qian, C., Fu, C. & Wu, Z. Changes in the amplitude of the temperature annual cycle in China and their implication for climate change research. *J. Clim.* **24**, 5292–5302 (2011).
- Xie, S. P. Interaction between the annual and interannual variations in the equatorial Pacific. *J. Phys. Oceanogr.* **25**, 1930–1941 (1995).
- Wu, Z. et al. The modulated annual cycle: an alternative reference frame for climate anomalies. *Clim. Dyn.* **31**, 823–841 (2008).
- Qian, C., Wu, Z., Fu, C. & Wang, D. On changing El Niño: a view from time-varying annual cycle, interannual variability, and mean state. *J. Clim.* **24**, 6486–6500 (2011).

14. Kharin, V. V., Zwiers, F. W., Zhang, X. & Hegerl, G. C. Changes in temperature and precipitation extremes in the IPCC ensemble of global coupled model simulations. *J. Clim.* **20**, 1419–1444 (2007).
15. Kharin, V. V. et al. Risks from climate extremes change differently from 1.5 C to 2.0 C depending on rarity. *Earth's Future* **6**, 704–715 (2018).
16. Li, C. et al. Changes in annual extremes of daily temperature and precipitation in CMIP6 models. *J. Clim.* **34**, 3441–3460 (2021).
17. IPCC AR6. Climate Change 2021: the physical science basis. Contribution of working group I to the sixth assessment report of the intergovernmental panel on climate change. Cambridge University Press 1513–1766 (2021).
18. Oliver, E. C. et al. Longer and more frequent marine heatwaves over the past century. *Nat. Commun.* **9**, 1–12 (2018).
19. Oliver, E. C. Mean warming not variability drives marine heatwave trends. *Clim. Dyn.* **53**, 1653–1659 (2019).
20. Sen Gupta, A. et al. Drivers and impacts of the most extreme marine heatwave events. *Sci. Rep.* **10**, 19359 (2020).
21. Parmesan, C. & Yohe, G. A globally coherent fingerprint of climate change impacts across natural systems. *Nature* **421**, 37–42 (2003).
22. Poloczanska, E. S. et al. Global imprint of climate change on marine life. *Nat. Clim. Change* **3**, 919–925 (2013).
23. Cavole, L. M. et al. Biological impacts of the 2013–2015 warm-water anomaly in the Northeast Pacific: winners, losers, and the future. *Oceanography* **29**, 273–285 (2016).
24. Wernberg, T. et al. Climate-driven regime shift of a temperate marine ecosystem. *Science* **353**, 169–172 (2016).
25. Smale, D. A. et al. Marine heatwaves threaten global biodiversity and the provision of ecosystem services. *Nat. Clim. Change* **9**, 306–312 (2019).
26. Frölicher, T. L. & Laufkötter, C. Emerging risks from marine heat waves. *Nat. Commun.* **9**, 1–4 (2018).
27. Yang, F. & Wu, Z. On the physical origin of the semiannual component of surface air temperature over oceans. *Clim. Dyn.* **59**, 2137–2149 (2022).
28. Rayner, N. A. et al. Global analyses of sea surface temperature, sea ice, and night marine air temperature since the late nineteenth century. *J. Geophys. Res. Atmos.* **108**, 4407–4435 (2003).
29. Hersbach, H. et al. The ERA5 global reanalysis. *Q. J. R. Meteorol. Soc.* **146**, 1999–2049 (2020).
30. Eyring, V. et al. Overview of the Coupled Model Intercomparison Project Phase 6 (CMIP6) experimental design and organization. *Geosci. Model Dev.* **9**, 1937–1958 (2016).
31. Qian, C. & Zhang, X. Changes in temperature seasonality in China: Human influences and internal variability. *J. Clim.* **32**, 6237–6249 (2019).
32. Feng, X., Qian, C. & Materia, S. Amplification of the temperature seasonality in the Mediterranean region under anthropogenic climate change. *Geophys. Res. Lett.* **49**, e2022GL099658 (2022).
33. Winton, M. Do climate models underestimate the sensitivity of Northern Hemisphere sea ice cover? *J. Clim.* **24**, 3924–3934 (2011).
34. Rosenblum, E. & Eisenman, I. Sea ice trends in climate models only accurate in runs with biased global warming. *J. Clim.* **30**, 6265–6278 (2017).
35. Jahn, A. Reduced probability of ice-free summers for 1.5 C compared to 2 C warming. *Nat. Clim. Change* **8**, 409–413 (2018).
36. Ding, Q. et al. Fingerprints of internal drivers of Arctic sea ice loss in observations and model simulations. *Nat. Geosci.* **12**, 28–33 (2019).
37. Topál, D. & Ding, Q. Atmospheric circulation-constrained model sensitivity recalibrates Arctic climate projections. *Nat. Clim. Change* **13**, 710–718 (2023).

Acknowledgements

This study is supported by the US National Science Foundation grant AGS-2307335.

Author contributions

Fucheng Yang and Zhaohua Wu contributed to the design and implementation of the research, to the analysis of the results and to the writing of the manuscript.

Competing interests

The authors declare no competing interests.

Additional information

Supplementary information The online version contains

supplementary material available at <https://doi.org/10.1038/s41612-024-00591-8>.

Correspondence and requests for materials should be addressed to Zhaohua Wu.

Reprints and permissions information is available at <http://www.nature.com/reprints>

Publisher's note Springer Nature remains neutral with regard to jurisdictional claims in published maps and institutional affiliations.

Open Access This article is licensed under a Creative Commons Attribution 4.0 International License, which permits use, sharing, adaptation, distribution and reproduction in any medium or format, as long as you give appropriate credit to the original author(s) and the source, provide a link to the Creative Commons licence, and indicate if changes were made. The images or other third party material in this article are included in the article's Creative Commons licence, unless indicated otherwise in a credit line to the material. If material is not included in the article's Creative Commons licence and your intended use is not permitted by statutory regulation or exceeds the permitted use, you will need to obtain permission directly from the copyright holder. To view a copy of this licence, visit <http://creativecommons.org/licenses/by/4.0/>.

© The Author(s) 2024